Li−Fe−P−O_2 Phase Diagram from First Principles Calculations

Shyue Ping Ong,† Lei Wang,† Byoungwoo Kang, and Gerbrand Ceder*

Department of Materials Science and Engineering, Massachusetts Institute of Technology, 77 Massachusetts Avenue, Cambridge, Massachusetts 02139

Received August 16, 2007. Revised Manuscript Received November 26, 2007

We present an efficient way to calculate the phase diagram of the quaternary Li−Fe−P−O_2 system using ab initio methods. The ground-state energies of all known compounds in the Li−Fe−P−O_2 system were calculated using the generalized gradient approximation (GGA) approximation to density functional theory (DFT) and the DFT+U extension to it. Considering only the entropy of gaseous phases, the phase diagram was constructed as a function of oxidation conditions, with the oxygen chemical potential, μ_{O_2}, capturing both temperature and oxygen partial pressure dependence. A modified Ellingham diagram was also developed by incorporating the experimental entropy data of gaseous phases. The phase diagram shows $LiFePO_4$ to be stable over a wide range of oxidation environments, being the first Fe^{2+}-containing phase to appear upon reduction at $\mu_{O_2} = -11.52$ eV and the last of the Fe-containing phosphates to be reduced at $\mu_{O_2} = -16.74$ eV. Lower μ_{O_2} represents more reducing conditions, which generally correspond to higher temperatures and/or lower oxygen partial pressures and/or the presence of reducing agents. The predicted phase relations and reduction conditions compare well to experimental findings on stoichiometric and Li-off-stoichiometric $LiFePO_4$. For Li-deficient stoichiometries, the formation of iron phosphate phases ($Fe_7(PO_4)_6$ and Fe_2 P_2O_7) commonly observed under moderately reducing conditions during $LiFePO_4$ synthesis and the formation of iron phosphides (Fe_2P) under highly reducing conditions are consistent with the predictions from our phase diagram. Our diagrams also predict the formation of Li_3PO_4 and iron oxides for Li-excess stoichiometries under all but the most reducing conditions, again in agreement with experimental observations. For stoichiometric $LiFePO_4$, the phase diagram gives the correct oxidation products of $Li_3Fe_2(PO_4)_3$ and Fe_2O_3. The predicted carbothermal reduction temperatures for $LiFePO_4$ from the Ellingham diagram are also within the range observed in experiments (800–900 °C). The diagrams developed provide a better understanding of phase relations within the Li−Fe−P−O_2 system and serve as a guide for future experimental efforts in materials processing, in particular, for the optimization of synthesis routes for $LiFePO_4$.

1. Introduction

In recent years, lithium transition metal phosphates have emerged as promising cathodes for rechargeable lithium batteries.[1–5] Of these, olivine $LiFePO_4$ has garnered the most interest because of its reasonable theoretical capacity of 170 mA h g^{-1}, low materials cost, and low toxicity. Because of its substantial potential, much research effort has been directed toward optimizing synthesis routes for $LiFePO_4$ cathodes. A variety of techniques have been developed to control particle size and morphology as well as improve the electrical conductivity of the electrode through coating with conducting phases (e.g., carbon or metallic iron phosphides) or aliovalent doping. One of the first attempts to dope $LiFePO_4$ with aliovalent cations was reported by Chung et al.[6] in 2002, who found that $Li_{0.99}Nb_{0.01}FePO_4$ densified at 800 °C formed black p-type conductors leading to a 6–7 orders of magnitude improvement in conductivity. However, subsequent investigations into aliovalent doping of $LiFePO_4$ by Herle et al.[7] and Delacourt et al.[8] found no evidence of an aliovalently doped structure. Though both reported the same increase in conductivity, they attributed the increase to a percolating network of iron phosphides and phosphocarbides believed to be formed from carbothermal reduction of $LiFePO_4$ or $Fe_2P_2O_7$. These findings were further supported by atomic scale investigations carried out by Islam et al.[9] which found $LiFePO_4$ to be intolerant of aliovalent doping on either the Li or Fe sites. More recently, Rho et al.[10] used a combination of Mössbauer and X-ray photoelectron spectroscopy to show that, under most synthesis conditions in inert or reducing atmospheres, FeP and Fe_2P,

* To whom correspondence should be addressed: Tel (617) 253-1581, Fax (617) 258-6534, e-mail gceder@mit.edu.
† These authors contribute equally to this work.

(1) Padhi, A. K.; Nanjundaswamy, K. S.; Goodenough, J. B. *J. Electrochem. Soc.* **1997**, *144*, 1188–1194.
(2) Huang, H.; Yin, S. C.; Nazar, L. F. *Electrochem. Solid State Lett.* **2001**, *4*, A170–A172.
(3) Morcrette, M.; Wurm, C.; Masquelier, C. *Solid State Sci.* **2002**, *4*, 239–246.
(4) Barker, J.; Saidi, M. Y.; Swoyer, J. L. *Electrochem. Solid State Lett.* **2003**, *6*, A53–A55.
(5) Morgan, D.; Ceder, G.; Saidi, M. Y.; Barker, J.; Swoyer, J.; Huang, H.; Adamson, G. *J. Power Sources* **2003**, *119*, 755–759.
(6) Chung, S. Y.; Bloking, J. T.; Chiang, Y. M. *Nat. Mater.* **2002**, *1*, 123–128.
(7) Herle, P. S.; Ellis, B.; Coombs, N.; Nazar, L. F. *Nat. Mater.* **2004**, *3*, 147–52.
(8) Delacourt, C.; Wurm, C.; Laffont, L.; Leriche, J. B.; Masquelier, C. *Solid State Ionics* **2006**, *177*, 333–341.
(9) Islam, M. S.; Driscoll, D. J.; Fisher, C. A. J.; Slater, P. R. *Chem. Mater.* **2005**, *17*, 5085–5092.
(10) Rho, Y. H.; Nazar, L. F.; Perry, L.; Ryan, D. *J. Electrochem. Soc.* **2007**, *154*, A283–A289.

10.1021/cm702327g CCC: $40.75
Published on Web 02/07/2008

along with Li_3PO_4, are formed on the surface via surface reduction at temperatures as low as 600 °C. Ellis et al.[11] also recently investigated the impact of synthesis conditions on the conductivity and electrochemical performance of various lithium transition metal phosphates. They found that using H_2 or NH_3 gas as a reducing agent, they were able to achieve the reduction of Li-deficient $LiFePO_4$ to iron phosphides at lower temperatures and shorter sintering periods than when using carbon alone. They claimed that this reduced particle growth and carbon consumption, thereby significantly improving electrochemical performance.

We can see, therefore, that a key factor to optimizing synthesis approaches for $LiFePO_4$ is a thorough understanding of phase equilibria under stoichiometric and off-stoichiometric conditions. $LiFePO_4$ is typically synthesized under highly reducing conditions to avoid the formation of Fe^{3+}. Often, an excess of lithium is introduced to compensate for its high volatility. Depending on the precursors used (e.g., carbon containing or otherwise), the exact synthesis environment (temperatures, Ar or N_2/H_2 atmosphere), and the degree and nature of off-stoichiometry, different secondary phases may be formed in addition to $LiFePO_4$, during either synthesis or subsequent reoxidation under normal operating conditions. The nature of such "impurity" phases can have a significant impact on the performance of the electrode. The presence of undesirable or inactive phases may at best reduce the capacity of the electrode and at worst seriously degrade electrochemical performance. On the other hand, some secondary phases may improve the performance of the electrode, for instance, by acting as electron conduits to compensate for the low intrinsic electrical conductivity of $LiFePO_4$.

There is currently no phase diagram available for the Li−Fe−P−O_2 system. Phase diagrams representing the thermodynamic phase equilibria of multicomponent systems reveal fundamental material aspects regarding the processing and reactions of materials. A Li−Fe−P−O_2 phase diagram would therefore provide useful insights into experimental findings on $LiFePO_4$ and also serve as a guide for future experimental efforts to optimize synthesis approaches for $LiFePO_4$. In this work, we have constructed the phase diagram for the quaternary Li−Fe−P−O_2 system as a function of oxidation conditions using first principles techniques. Using the information on phase relations garnered from the phase diagram, we were then able to construct an Ellingham-type diagram for reactions of interest using a combination of total energies obtained from first principles calculations and experimental entropy data of gaseous phases.

2. Methodology

2.1. Free Energy Model. To construct a phase diagram, one would need to compare the relative thermodynamic stability of phases belonging to the system using an appropriate free energy model. For an isothermal, isobaric, closed Li−Fe−P−O_2 system, the relevant thermodynamic potential is the Gibbs free energy, G, which can be expressed as a Legendre transform of the enthalpy, H, and internal energy, E, as follows:

$$G(T,P,N_{Li},N_{Fe},N_P,N_{O_2}) = H(T,P,N_{Li},N_{Fe},N_P,N_{O_2}) - TS(T,P,N_{Li},N_{Fe},N_P,N_{O_2}) = E(T,P,N_{Li},N_{Fe},N_P,N_{O_2}) + PV(T,P,N_{Li},N_{Fe},N_P,N_{O_2}) - TS(T,P,N_{Li},N_{Fe},N_P,N_{O_2}) \quad (2.1)$$

where T is the temperature of the system, S is the entropy of the system, P is the pressure of the system, V is the volume of the system, and N_i is the number of atoms of species i in the system.

In the Li−Fe−P−O_2 system, we are primarily comparing the relative stability of condensed phases, for which $P\Delta V$ is generally small and the PV term may therefore be neglected. At 0 K, the expression for G simplifies to just E. Normalizing E with respect to the total number of particles in the system, we obtain $\bar{E}(0,P,x_{Li},x_{Fe},x_P,X_{O_2})$, where $x_i = N_i/(N_{Li} + N_{Fe} + N_P + N_{O_2})$. By taking the convex hull[12] of $\bar{E}$ for all phases belonging to the M-component system and projecting the stable nodes into the $(M - 1)$-dimension composition space, one can obtain the 0 K phase diagram for the closed system at constant pressure. The convex hull of a set of points is the smallest convex set containing the points. For instance, to construct a 0 K, closed Li−Fe−P−O_2 system phase diagram, the convex hull is taken on the set of points in ($\bar{E}$, x_{Li}, x_{Fe}, x_P) space with x_{O_2} being related to the other three composition variables by $x_{O_2} = 1 - x_{Li} - x_{Fe} - x_P$.

2.2. Determining E from Density Functional Theory. In this work, we have extracted all known ordered compounds in the Inorganic Crystal Structure Database (ICSD)[13] belonging to the quaternary Li−Fe−P−O_2 system and calculated the energies for these using the generalized gradient approximation (GGA) to density functional theory (DFT) and the GGA+U extension to it. Projected augmented wave (PAW)[14] pseudopotentials were used, as implemented in the Vienna Ab initio Simulation Package (VASP).[15] An energy cutoff of 500 eV and appropriate k-point meshes were chosen so that total energies converged within 3 meV per formula unit with the atomic positions and lattice vectors fully relaxed. All calculations were spin-polarized, but no attempt was made to find antiferromagnetic solutions except for the iron oxides for which the magnetic ground states are well-known.

The DFT+U methodology was chosen for its appropriateness for the redox reactions studied in this work. It is well-known that first principles calculations within the local density approximation (LDA) or GGA lead to considerable error in calculated redox energies of transition metal oxides. This arises from the self-interaction error in LDA and GGA, which is not canceled out in redox reactions where an electron is transferred between significantly different environments, such as between a metal and a transition metal or between a transition metal and oxygen. In 2004, Zhou et

(11) Ellis, B.; Herle, P. S.; Rho, Y. H.; Nazar, L. F.; Dunlap, R.; Perry, L. K.; Ryan, D. H. *Faraday Discuss.* **2007**, *134*, 119–141.

(12) Barber, C. B.; Dobkin, D. P.; Huhdanpaa, H. *ACM Trans. Math. Software* **1996**, *22*, 469–483.

(13) Fachinformationszentrum (FIZ) Karlsruhe, Inorganic Crystal Structure Database, http://icsdweb.fiz-karlsruhe.de/, 2007.

(14) Kresse, G.; Joubert, D. *Phys. Rev. B* **1999**, *59*, 1758–1775.

(15) Kresse, G.; Furthmuller, J. *Phys. Rev. B* **1996**, *54*, 11169–11186.

al.[16] demonstrated that a GGA+U treatment[17] of the localized d orbitals with an explicit Hubbard term to cancel the self-interactions led to significantly improved accuracy in the calculated redox energies and Li insertion voltages for lithium transition metal cathodes. Similarly, Wang et al.[18,19] showed the benefit of the U correction in improving the calculated oxidation energies for transition metal oxides. On the basis of these works, we have used a $U_{\text{effective}}$ value of 4.3 eV, which is the average of the self-consistently determined $U_{\text{effective}}$ values[16] for Fe^{2+} and Fe^{3+}. It should be noted, however, that the value of $U_{\text{effective}}$ tends to become smaller as the valence state of Fe decreases. Hence, the $U_{\text{effective}}$ value used may be somewhat too small for oxidized states (e.g., Fe_2O_3) and too large for reduced states (e.g., FeO). In particular, we expect considerable error in the calculated energies of metallic systems such as Fe metal and the iron phosphides, Fe_xP_y, where the d orbitals are no longer atomic-like and the GGA+U methodology is less applicable.

2.3. Phase Diagram Construction. The description of a closed four-component system at constant temperature and pressure requires three-dimensional space and can be represented in the form of a composition tetrahedron. However, given the large number of phases present in the Li−Fe−P−O_2 system, this representation is not one that is amenable to easy analysis. Furthermore, such a phase diagram, which describes phase equilibria in an environment with controlled Li, Fe, P, and O_2 compositions, is not reflective of the environments of interest.

The key control variable in the synthesis of $LiFePO_4$ is the oxygen chemical potential, μ_{O_2}. $LiFePO_4$ synthesis requires reducing environments, which are usually achieved using relatively high temperature processing (typically 600–850 °C) and a low oxygen environment such as an Ar or N_2 atmosphere. In some cases, even more extreme reducing environments are achieved with the presence of carbon or H_2 as reducing agents. In essence, the system of interest is an isothermal, isobaric system that is open with respect to oxygen and closed with respect to the other components, rather than a completely closed system. The relevant thermodynamic potential to study phase equilibria with respect to an oxidizing or reducing environment is the oxygen grand potential, defined as

$$\varphi(T,P,N_{\text{Li}},N_{\text{Fe}},N_{\text{P}},\mu_{O_2}) = G(T,P,N_{\text{Li}},N_{\text{Fe}},N_{\text{P}},\mu_{O_2}) - \mu_{O_2}N_{O_2}(T,P,N_{\text{Li}},N_{\text{Fe}},N_{\text{P}},\mu_{O_2}) \quad (2.2)$$

$$\approx E(T,P,N_{\text{Li}},N_{\text{Fe}},N_{\text{P}},\mu_{O_2}) - TS(T,P,N_{\text{Li}},N_{\text{Fe}},N_{\text{P}},\mu_{O_2}) - \mu_{O_2}N_{O_2}(T,P,N_{\text{Li}},N_{\text{Fe}},N_{\text{P}},\mu_{O_2}) \quad (2.3)$$

where the PV term is again ignored.

Normalizing φ with respect to Li−Fe−P composition and dropping the explicit expression of the functional dependence of E, S, and N_{O_2} on the right-hand side henceforth for brevity, we obtain

$$\bar{\varphi}(T,P,x_{\text{Li}},x_{\text{Fe}},x_{\text{P}},\mu_{O_2}) \approx \frac{E - TS - \mu_{O_2}N_{O_2}}{N_{\text{Li}} + N_{\text{Fe}} + N_{\text{P}}} \quad (2.4)$$

where $x_i = N_i/(N_{\text{Li}} + N_{\text{Fe}} + N_{\text{P}})$ is the fraction of component i in Li−Fe−P composition space.

To formally introduce temperature into ab initio phase stability calculations, one would usually need to take into account all the relevant excitations (e.g., vibrational, configurational, and electronic) that contribute to entropy.[20–24] However, for our chosen system, a few simplifying assumptions can be made that allow us to obtain a useful approximate phase diagram with less effort. For an open system with respect to oxygen, phase equilibria changes take place primarily through reactions involving the absorption or loss of oxygen gas. In such reactions, the reaction entropy is dominated by the entropy of oxygen gas, and the effect of temperature is mostly captured by changes in the oxygen chemical potential. The oxygen chemical potential is related to the temperature and oxygen partial pressure by the following equations:

$$\mu_{O_2}(T,p_{O_2}) = \mu_{O_2}(T,p_0) + kT\ln\frac{p_{O_2}}{p_0} \quad (2.5)$$

$$\approx h_{O_2}(T,p_0) - T\left(s_{O_2}(T,p_0) - k\ln\frac{p_{O_2}}{p_0}\right) \quad (2.6)$$

where p_{O_2} is the partial pressure of oxygen, p_0 is a reference oxygen partial pressure, which for this work is 0.1 MPa, $s_{O_2}(T,p_0)$ is the per molecule entropy of oxygen at the reference partial pressure and temperature T, $\mu_{O_2}(T,p_0)$ is the oxygen chemical potential at the reference partial pressure and temperature T, $h_{O_2}(T,p_0)$ is the per molecule oxygen enthalpy at the reference partial pressure and temperature T, and k is Boltzmann's constant.

Since the TS term in eq 2.4 is the entropy contribution to $\bar{\varphi}$ of the condensed system, it can be neglected compared to the entropy effect of μ_{O_2} on $\bar{\varphi}$ (due to the much larger contribution of $N_{O_2}s_{O_2}$ compared to S), and the expression for $\bar{\varphi}$ simplifies to

$$\bar{\varphi}(\mu_{O_2},x_{\text{Li}},x_{\text{Fe}},x_{\text{P}}) \approx \frac{E - \mu_{O_2}N_{O_2}}{N_{\text{Li}} + N_{\text{Fe}} + N_{\text{P}}} \quad (2.7)$$

Using the above assumption, the effect of temperature and oxygen partial pressure can be fully captured in a single variable, μ_{O_2}, with a more negative value corresponding to higher T or lower p_{O_2} (as can be seen from eq 2.6).

Varying μ_{O_2}, the Li−Fe−P−O_2 phase diagram can be constructed as constant μ_{O_2} sections in (μ_{O_2}, x_{Li}, x_{Fe}, x_{P}) space by taking the convex hull of $\bar{\varphi}$ for all phases at a particular μ_{O_2} and projecting the stable nodes onto a two-dimensional Li−Fe−P Gibbs triangle. Each constant μ_{O_2} phase diagram then represents phase equilibria at a particular oxidation

(16) Zhou, F.; Cococcioni, M.; Marianetti, C. A.; Morgan, D.; Ceder, G. *Phys. Rev. B* **2004**, *70*, 235121.
(17) Anisimov, V. I.; Aryasetiawan, F.; Lichtenstein, A. I. *J. Phys.: Condens. Matter* **1997**, *9*, 767–808.
(18) Wang, L.; Maxisch, T.; Ceder, G. *Phys. Rev. B* **2006**, *73*, 195107.
(19) Wang, L.; Maxisch, T.; Ceder, G. *Chem. Mater.* **2007**, *19*, 543–552.
(20) Sanchez, J. M.; Fontaine, D. D. *Phys. Rev. B* **1978**, *17*, 2926–2936.
(21) Asta, M.; McCormack, R.; DeFontaine, D. *Phys. Rev. B* **1993**, *48*, 748–766.
(22) Kohan, A. F.; Tepesch, P. D.; Ceder, G.; Wolverton, C. *Comput. Mater. Sci.* **1998**, *9*, 389–396.
(23) Garbulsky, G. D.; Ceder, G. *Phys. Rev. B* **1994**, *49*, 6327–6330.
(24) Ackland, G. J. *J. Phys.: Condens. Matter* **2002**, *14*, 2975–3000.

environment, and each point in the phase diagram provides the phase or combination of phases with the lowest $\bar{\varphi}$.

2.4. Modified Ellingham Diagram Construction. The effective oxygen partial pressure may be affected by the presence of reducing or oxidizing agents. For example, to improve electrical conductivity, carbon-containing precursors are often used in the synthesis of $LiFePO_4$. Carbon is a reducing agent, and carbothermal reduction (CTR) is used extensively to reduce metal oxides to metals. The preparation of $LiFePO_4$ using CTR has been carried by various groups since it was first reported by Barker et al. in 2003.[4]

Carbon oxidation during CTR can take place via two different reactions:

$$C + O_2 \rightleftharpoons CO_2$$

$$2C + O_2 \rightleftharpoons 2CO$$

The CO_2 reaction, which is more thermodynamically favorable at lower temperatures, has minimal volume change and hence negligible entropy change. At temperatures in excess of 1000 K, however, the formation of CO becomes more thermodynamically favorable than the CO_2 reaction.[25] The CO reaction creates one extra mole of gas for every mole of oxygen consumed and therefore involves an increase in entropy. As temperature increases, the free energy of formation of CO becomes increasingly negative, and this leads to stronger reducing conditions. In this work, we will primarily focus on the CO reaction since $LiFePO_4$ synthesis is usually conducted at relatively high temperatures. Another reducing agent commonly used in $LiFePO_4$ synthesis is hydrogen gas, which is oxidized according to the following reaction:

$$2H_2 + O_2 \rightleftharpoons 2H_2O$$

For metal oxides, a typical method of showing the relationship between the reduction transition temperatures, oxygen partial pressures, and the presence of reducing agents is an Ellingham diagram,[26] which shows the change in free energy of the oxidation reaction as a function of temperature. In this work, we have used a modified Ellingham construction where the change in Gibbs free energy for reduction reactions of interest (normalized to a per O_2 molecule basis) in the $Li−Fe−P−O_2$ system is plotted against temperature.

Consider the following general reaction:

$$\text{condensed reactants} + \text{gaseous reactants} \rightleftharpoons \text{condensed products} + \text{gaseous products}$$

where the gaseous products can be O_2, CO, or H_2O depending on whether the reaction is a thermal reduction, carbothermal reduction, or hydrogen reduction, respectively, and the gaseous reactant comprises H_2 in the case of hydrogen reduction. As the entropy contributions of gases are much higher than that of condensed phases, the change in Gibbs free energy of the reaction can then be approximated as follows:

$$\Delta G = G_{\text{products}} - G_{\text{reactants}} \tag{2.8}$$

$$\approx H_{\text{products}} - H_{\text{reactants}} - T(S_{\text{gaseous products}} - S_{\text{gaseous reactants}}) \tag{2.9}$$

where the enthalpy, H, can be approximated with the internal energy, E, at 0 K.

To determine ΔG, we have used the energies for the various phases from our DFT calculations and experimental entropy values for the gases. For the 0 K energy of O_2 gas, earlier work by Wang et al.[18] has shown that one of the main sources of error in calculating the redox reaction enthalpies of transition metal oxides is related to the GGA error in the energy associated with the formation of O^{2-} ions from O_2 molecules and vice versa. It is believed that this error arises from the well-known overbinding of O_2 molecule in GGA as well as an additional GGA error associated with adding electrons to the oxygen p orbital when O^{2-} is formed from O_2. Wang et al. estimated that this error can be corrected through a constant shift of −1.36 eV per O_2 molecule, which also includes the $P\Delta V$ contribution to the oxygen enthalpy. For the purposes of this work, we have applied this same shift to the calculated energy of the O_2 molecule. Experimental thermodynamic data for O_2, CO, H_2, and H_2O at 0.1 MPa were obtained from the JANAF thermochemical tables.[25] To further simplify the analysis, we have assumed that all other phases are in condensed form at the temperatures of interest, even though there may be some phases (e.g., phosphorus) that vaporize at fairly low temperatures.

3. Results

3.1. Calculated Energies. The calculated energies and structures of the compounds studied in this paper are presented in Table 1. All energies are presented as per formula unit (fu) formation energies, E_f, from the elements, Li, Fe, P, and O_2.

3.2. Phase Diagrams of Ternary Subsystems. To verify that the calculated energies reasonably reflect the relative stability of the various phases, we first constructed the phase diagrams of the various ternary subsystems at 0 K, i.e., the Li−P−O, Li−Fe−O, Fe−P−O, and Li−Fe−P systems, and compared these with known experimental phase diagrams for these systems.[27−31] It should be noted, however, that the experimental phase diagrams are generally for nonzero temperatures while the calculated phase diagrams represent phase equilibria at 0 K. Hence, some differences between the experimental and first principles phase diagrams are to be expected.

The phase diagrams constructed from first principles calculations are given in Figure 1. For the ternary diagrams

(25) Chase, M. W. *NIST-JANAF Thermochemical Tables*; American Institute of Physics: Woodbury, NY, 1998; Vol. 12.
(26) Ellingham, H. J. T. *J. Soc. Chem. Ind., London* **1944**, *63*, 125.
(27) Osterheld, R. K. *J. Inorg. Nucl. Chem.* **1968**, *30*, 3174.
(28) Raghavan, V. *Phase Diagrams of Binary Iron Alloys*; Indian Institute of Metals: Salt Lake City, Kolkata, 1989.
(29) Modaressi, A.; Kaell, J. C.; Malaman, B.; Gerardin, R.; Gleitzer, C. *Mater. Res. Bull.* **1983**, *18*, 101–109.
(30) Villars, P.; Prince, A.; Okamoto, H. *Handbook of Ternary Alloy Phase Diagrams*; ASM Int.: Tokyo, 1995; Vol. 8, pp 10378–10379.
(31) Okamoto, H. *Phase Diagrams of Binary Iron Alloys*; ASM Int.: Tokyo, 1993.

Table 1. Crystal Structures and Calculated Formation Energies of Phases in the Li−Fe−P−O_2 System

phase	crystal structure	E_f (eV[a])	phase	crystal structure	E_f (eV)
Li_2O	$Fm\bar{3}m$	−6.200	$LiFeO_2$	$R\bar{3}m$	−9.156
Li_2O_2	$P6_3/mmc$	−7.040	Li_5FeO_4	$Pbca$	−21.883
FeO	$Fm\bar{3}m$	−4.095	Li_3PO_4	$Pnma$	−22.189
Fe_2O_3	$R\bar{3}c$	−11.250	$Li_4P_2O_7$	$P2_1/c1$	−36.022
Fe_3O_4	$Fd\bar{3}m$	−15.682	$LiPO_3$	$P2/c$	−13.685
Fe_3P	$I\bar{4}$	−1.114	$Fe_9(PO_4)O_8$	$Cmmm$	−47.628
Fe_2P	$Pnnm$	−0.876	$Fe_3(PO_4)O_3$	$R3m$	−26.078
FeP	$Pnma$	−0.339	$Fe_4(PO_4)_2O$	$P2_1/c$	−38.360
FeP_2	$P\bar{6}2m$	−0.601	Fe_2PO_4O	$Pnma$	−20.143
FeP_4	$P2_1/c$	−1.265	$Fe_3(PO_4)_2$	$P2_1/c$	−34.187
P_4O_{18}	$P2_12_12_1$	−32.042	$Fe_7(PO_4)_6$	$P\bar{1}$	−95.984
P_2O_5	$Pnma$	−17.343	$Fe_2P_2O_7$	$C\bar{1}$	−29.097
P_4O_9	$R\bar{3}c$	−31.265	$FePO_4$	$Pnma$	−15.309
$(P_4O_6)O_2$	$C2/c$	−27.792	$Fe_7(P_2O_7)_4$	$C222_1$	−113.022
P_4O_7	$P2_1/c$	−24.028	$Fe_3(P_2O_7)_2$	$Pnma$	−55.034
P_4O_6	$P2_1/m$	−20.173	$Fe_4(P_2O_7)_3$	$P2_1/c$	−80.173
LiP_7	$I4_1/acd$	−2.261	$Fe_2P_4O_{12}$	$C2/c$	−47.801
LiP_5	$Pna2_1$	−1.873	$Fe(PO_3)_3$	Cc	−33.953
LiP	$P2_1/c$	−1.193	FeP_4O_{11}	$C\bar{1}$	−41.533
Li_3P_7	$P2_12_12_1$	−4.619	$LiFePO_4$	$Pnma$	−18.853
Li_3P	$P6_3/mmc$	−2.944	$Li_3Fe_2(PO_4)_3$	$P2_1/c$	−53.192
LiFeP	$P4/nmm$	−1.238	$LiFeP_2O_7$	$P2_1$	−29.376
$LiFe_5O_8$	$P4_332$	−30.650	$LiFeP_3O_9$	$P2_12_12_1$	−37.523
$Li_3Fe_5O_8$	$P4_332$	−35.668	$Li_9Fe_3(P_2O_7)_3(PO_4)_2$	$P\bar{3}c1$	−132.471

[a] 1 eV/fu = 96.49 kJ/mol = 23.06 kcal/mol.

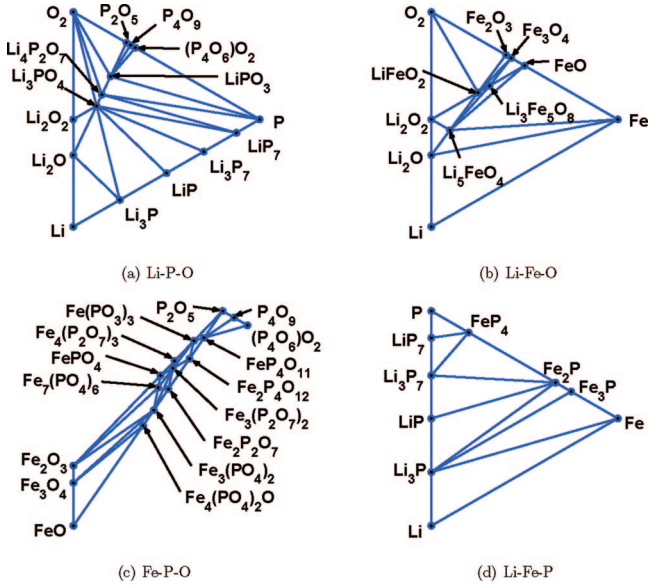

Figure 1. Phase diagrams for ternary subsystems. Only the section of the Fe−P−O phase diagram bounded by the oxides is shown given the large number of phases in this system.

with oxygen as a component, the reference O_2 energy used includes the constant −1.36 eV correction to the oxygen enthalpy mentioned previously. This reference energy has no effect on the constant μ_{O_2} phase diagram but only modifies the scale of the oxygen chemical potential. Comparing the experimental and calculated diagrams, the following key observations can be made:

1. Li−P−O System. All compounds present in the experimental $Li_2O-P_2O_5$ phase diagram at 500 °C[27] are present in our calculated diagrams. Of the five known Li−P binary phases,[32] LiP_7, LiP, Li_3P, and Li_3P_7 are present in our phase diagram while LiP_5 is only slightly above the convex hull.

2. Li−Fe−O System. Our phase diagram correctly reflects the stable compounds of $LiFeO_2$ and Li_5FeO_4 in the experimental diagram at 400 °C.[28] However, instead of $LiFe_5O_8$, the lithiated form, $Li_3Fe_5O_8$, is present in our phase diagram.

3. Fe−P−O System. The experimental Fe−P−O phase diagram for Fe/P ≥ 1 at 900 °C has been established by Modaressi et al.[29] Of the nine ternary phases identified by Modaressi in this region, five are present in our calculated phase diagram ($Fe_3(PO_4)_2$, $Fe_4(PO_4)_2O$, $Fe_2P_2O_7$, $Fe_7(PO_4)_6$, and $FePO_4$). $Fe_3(PO_4)O_3$, $Fe_2(PO_4)O$, and $Fe_9(PO_4)O_8$ are present in the experimental diagram but not present in our calculated diagram, even though these phases were considered in our calculations. The experimental diagram also identifies $Fe_5(PO_4)_3O$ to be a stable phase, though this phase was not included in our computations as it is not in the ICSD database. For Fe/P < 1, our calculated phase diagram identifies $Fe_3(P_2O_7)_2$, $Fe_4(P_2O_7)_3$, FeP_4O_{11}, $Fe_2P_4O_{12}$, and $Fe(PO_3)_3$ to be stable phases.

4. Li−Fe−P System. Compared with the experimental Li−Fe−P phase diagram at 800 °C,[30] the binary Li_3P, LiP, Fe_3P, and Fe_2P phases are present in our calculated diagram. However, FeP and the only known ternary phase, LiFeP[33,34] are not stable phases in our calculated phase diagram. Compared with the experimental binary Fe−P phase diagram,[31] all the iron phosphide phases are present in our calculated diagram except FeP and FeP_2. As mentioned in the previous section, we expect significant errors in the calculated energies of metallic phases such as Fe metal and the iron phosphides as the GGA+U methodology is less applicable. Indeed, using GGA

(32) Sangster, J.; Pelton, A.; Okamoto, H. *J. Phase Equilib. Diffus.* **1995**, *16*, 92–93.

(33) Juza, R.; Langer, K. *Z. Anorg. Allg. Chem.* **1968**, *361*, 58–73.

(34) Boyanov, S.; Bernardi, J.; Gillot, F.; Dupont, L.; Womes, M.; Tarascon, J. M.; Monconduit, L.; Doublet, M. L. *Chem. Mater.* **2006**, *18*, 3531–3538.

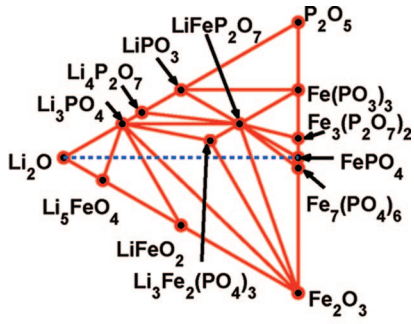

(a) $\mu_{O_2} = -10.50\ eV$, $Fe_7(PO_4)_6$ appears

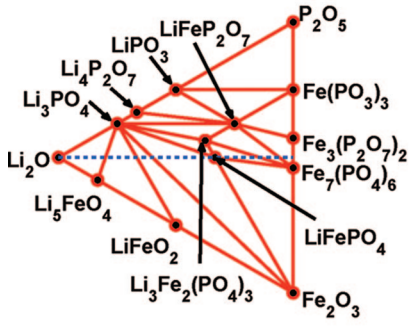

(b) $\mu_{O_2} = -11.52\ eV$, $LiFePO_4$ appears

Figure 2. Phase diagrams at less reducing environments.

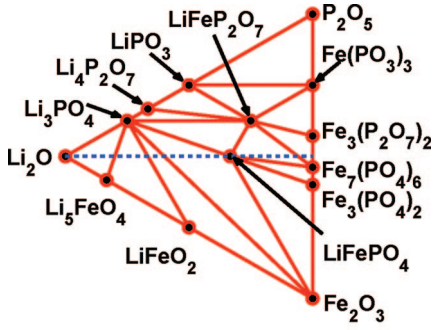

(a) $\mu_{O_2} = -11.74\ eV$, $Li_3Fe_2(PO_4)_3$ disappears

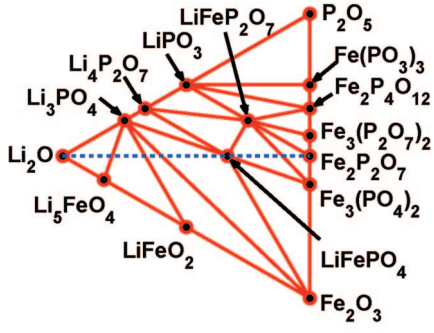

(b) $\mu_{O_2} = -12.38\ eV$, $Fe_2P_2O_7$ appears

Figure 3. Phase diagrams at more reducing environments.

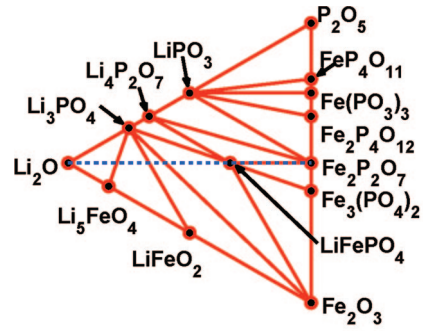

(a) $\mu_{O_2} = -13.08\ eV$, $LiFeP_2O_7$ disappears

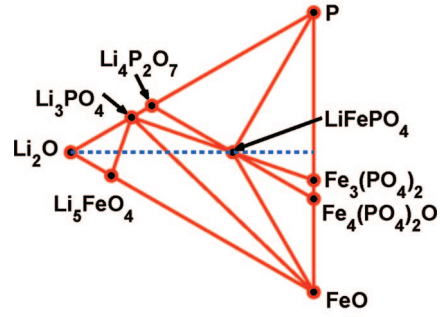

(b) $\mu_{O_2} = -16.08\ eV$, $Fe_2P_2O_7$ disappears

Figure 4. Phase diagrams at highly reducing environments.

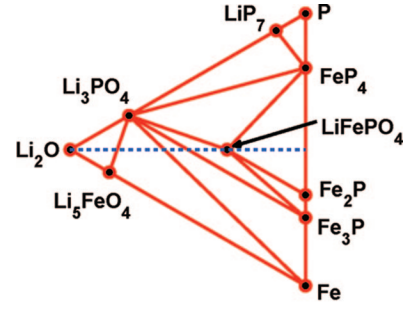

(a) $\mu_{O_2} = -16.70\ eV$, $Fe_3(PO_4)_2$ disappears

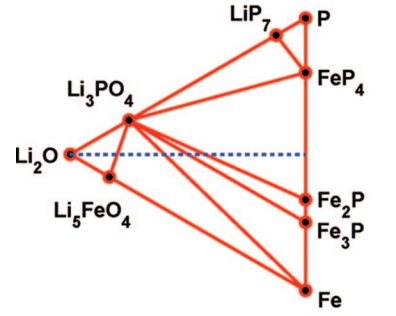

(b) $\mu_{O_2} = -16.74eV$, $LiFePO_4$ disappears

Figure 5. Phase diagrams at extremely reducing environments.

energies (without the +U extension) results in a Li−Fe−P phase diagram (not shown) which is more consistent with the experimental diagram. With the exception of Fe_3P, all other phases present in the experimental diagram are present in the GGA phase diagram. However, the +U extension is necessary to obtain accurate redox energies for the iron oxide and phosphate phases, which are the phases of interest in this work. Hence, GGA+U energies of all phases were used in constructing the phase diagram.

3.3. Constant μ_{O_2} Phase Diagrams. Using the calculated energies and the methodology outlined earlier, we have constructed a series of phase diagrams at constant μ_{O_2}, given in Figures 2−5. Diagrams at lower μ_{O_2} represent more reducing environments, which correspond to higher temperatures and/or lower oxygen partial pressures and/or the

presence of reducing agents, while higher μ_{O_2} represents less reducing environments. The values of μ_{O_2} are chosen so as to present diagrams at key transition μ_{O_2}, i.e., values of μ_{O_2} where an important phase of interest (say $LiFePO_4$) is formed or removed. Figure 2 shows diagrams at mildly reducing environments in which the monoclinic $Li_3Fe_2(PO_4)_3$ phase is still present and most Fe-containing phases have Fe in the 3+ oxidation state. At $\mu_{O_2} = -11.52$ eV, $LiFePO_4$ appears as the first stable Fe^{2+}-containing phase. As the environment becomes more reducing, phases containing Fe^{3+} are progressively being reduced to Fe^{2+}. Figure 3 shows phase diagrams where mixed valence phosphates, such as $Fe_7(PO_4)_6$, are being reduced to Fe^{2+} phases. At even more reducing environments (Figure 4), Fe^{2+} becomes the dominant valence state for Fe. Finally, at the extremely reducing environments represented by Figure 5, the iron phosphates are reduced to the metallic iron phosphides (Fe valence of 0), and eventually $LiFePO_4$ itself is reduced. The reduction of the remaining highly stable oxygen-containing phases (Li_3PO_4 and Li_2O) takes place at conditions much more reducing than those of interest in this paper. Under those conditions, the ternary Li−Fe−P phase (Figure 1d) is reproduced.

Also plotted in all the phase diagrams are dotted lines representing the path of Li off-stoichiometry with respect to $LiFePO_4$. Compositions to the left of $LiFePO_4$ have Li excess while compositions to the right have Li deficiency. For compositions that do not lie at a stable node on the phase diagram, the phases in equilibrium are given by the vertices of the triangle bounding the position of that composition. For instance, at $\mu_{O_2} = -16.70$ eV, the phase diagram indicates that a Li-deficient material ($Li_{1-x}FePO_4$) material will consist of $LiFePO_4$, FeP_4, and Fe_2P.

3.4. Modified Ellingham Diagram. From the phase diagrams, we were able to extract the predicted phase relations for key reactions of interest. For instance, from the phase diagrams in Figures 2 and 3, we can see that a system with a Li:Fe:P composition of 3:2:3 will transit from a single phase, $Li_3Fe_2(PO_4)_3$, to a mixture of $LiFePO_4$, Li_3PO_4, and $LiFeP_2O_7$ as μ_{O_2} decreases; i.e., $Li_3Fe_2(PO_4)_3$ is being reduced to $LiFePO_4$, Li_3PO_4, and $LiFeP_2O_7$ with the release of O_2.

On the basis of calculated phase diagrams, we have constructed the modified Ellingham diagram presented in Figure 6. The reactions chosen are those in which a phase of interest is being reduced or is being formed via a reduction reaction (e.g., formation and reduction of $LiFePO_4$). As these reduction reactions are not thermodynamically favored at 0 K, the changes in free energy of the reactions are positive and decrease as temperature increases due to the entropy associated with the release of oxygen gas.

The estimated transition temperatures for thermal reduction at the reference oxygen partial pressure of 0.1 MPa are given by the intercept of the reaction lines (labeled 1–9 in Figure 6) with the temperature axis. At the transition temperature, the ΔG of a reaction changes from positive to negative and the reaction becomes thermodynamically favorable. The thermal reduction temperatures at lower oxygen partial pressures can be found where the $\Delta G(T)$ line intersects the relevant P_{O_2} line. Finally, the transition temperature for

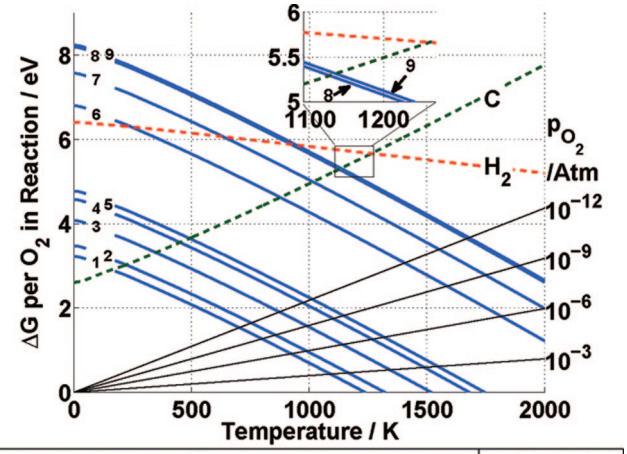

Reaction	Line Label
$3\ Li_3Fe_2(PO_4)_3 \rightleftharpoons 4\ LiFePO_4 + 2\ LiFeP_2O_7 + Li_3PO_4 + O_2$	1
$\frac{3}{2}\ Fe_7(PO_4)_6 \rightleftharpoons Fe_3(P_2O_7)_2 + \frac{5}{2}\ Fe_3(PO_4)_2 + O_2$	2
$2\ Fe_3(P_2O_7)_2 \rightleftharpoons 2\ Fe_2P_2O_7 + Fe_2P_4O_{12} + O_2$	3
$4\ LiFeP_2O_7 \rightleftharpoons 4\ LiPO_3 + 2\ Fe_2P_2O_7 + O_2$	4
$6\ Fe_2O_3 \rightleftharpoons 4\ Fe_3O_4 + O_2$	5
$2\ Fe_3O_4 \rightleftharpoons 6\ FeO + O_2$	6
$\frac{6}{5}\ Fe_2P_2O_7 \rightleftharpoons \frac{4}{5}\ Fe_3(PO_4)_2 + \frac{4}{5}\ P + O_2$	7
$2\ FeO \rightleftharpoons 2\ Fe + O_2$	8
$\frac{1}{4}\ Fe_3(PO_4)_2 \rightleftharpoons \frac{1}{28}\ FeP_4 + \frac{5}{14}\ Fe_2P + O_2$	
$\frac{3}{4}\ LiFePO_4 \rightleftharpoons \frac{1}{4}\ Li_3PO_4 + \frac{5}{14}\ Fe_2P + \frac{1}{28}\ FeP_4 + O_2$	9
$2CO \rightleftharpoons 2C + O_2$	C
$2H_2O \rightleftharpoons 2H_2 + O_2$	H_2

Figure 6. Modified Ellingham diagram for reduction reactions in the Li−Fe−P−O_2 system.

reduction by C/CO-CTR or hydrogen reduction at the reference partial pressure is given by the temperatures which the $\Delta G(T)$ line intersects the C or H_2 line.

The iron oxide reactions are included as a useful reference for comparison with the widely available Ellingham diagram for the metal oxides. The predicted C/CO-CTR transition temperatures for FeO → Fe, Fe_3O_4 → FeO, and Fe_2O_3 → Fe_3O_4 are approximately 1130, 880, and 490 K, respectively, which compares reasonably well to the experimental values of approximately 990, 930, and 540 K.

4. Discussion

4.1. Phase Equilibria Pertinent to $LiFePO_4$ Synthesis. One of our key motivations for fully characterizing the Li−Fe−P−O_2 phase diagram is to apply these diagrams to understand how different synthesis conditions create $LiFePO_4$ with very different electrochemical performance. From Figures 2−5, we observe that olivine $LiFePO_4$ is stable over a wide range of oxidation environments. $LiFePO_4$ is the first Fe^{2+}-containing phase to appear at $\mu_{O_2} = -11.52$ eV and the last of the Fe-containing phosphates to be reduced at $\mu_{O_2} = -16.74$ eV. This large stability range provides a wide range of options for selecting the phases that can coexist with $LiFePO_4$.

In recent years, various research groups have experimented with synthesis approaches for $LiFePO_4$ in which Li off-stoichiometry is introduced under a variety of reducing environments. The aim is to achieve phase equilibria in which conducting phases (e.g., iron phosphides) are formed together with $LiFePO_4$, thereby compensating for the low electrical

Table 2. Predicted Phase Equilibria under Various Oxidation and Li Off-Stoichiometry Conditions

μ_{O_2}/eV	Li-deficient	stoichiometric	Li-excess
−10.50	severe deficiency: $LiFeP_2O_7 + FePO_4 + Fe_7(PO_4)_6$ intermediate deficiency: $LiFeP_2O_7 + Fe_2O_3 + Fe_7(PO_4)_6$ slight deficiency: $Li_3Fe_2(PO_4)_3 + LiFeP_2O_7 + Fe_2O_3$	$Li_3Fe_2(PO_4)_3 + Fe_2O_3$	slight−intermediate excess: $Li_3Fe_2(PO_4)_3 + Li_3PO_4$
−13.08	$LiFePO_4 + Fe_2P_2O_7$	$LiFePO_4$	slight−intermediate excess: $LiFePO_4 + Li_3PO_4 + Fe_2O_3$
−16.70	$LiFePO_4 + FeP_4 + Fe_2P$	$LiFePO_4$	slight excess: $LiFePO_4 + Li_3PO_4 + Fe_3P$ intermediate excess: $Li_3PO_4 + Fe_3P + Fe$

conductivity for $LiFePO_4$. In three papers published between 2004 and 2007 (Herle et al.,[7] Rho et al.,[10] Ellis et al.[11]), Nazar and colleagues reported that the increase in conductivity previously attributed by Chung et al.[6] to aliovalent doping is in fact due to the formation of iron phosphides during $LiFePO_4$ synthesis. Systematic investigations were carried out on "Zr-doped" $Li_{1-x}Zr_{0.01}FePO_4$ (with the doping resulting in a Li deficiency), stoichiometric $LiFePO_4$, and undoped Li-deficient $LiFePO_4$ processed at temperatures ranging from 600 to 850 °C. They found that, regardless of doping, Li-deficient $Li_{1-x}FePO_4$ ($0.01 < x < 0.07$) formed $Fe_2P_2O_7$ at 600 °C, which disappeared at 800 °C to form Fe_2P and iron phosphocarbide, $Fe_{75}P_{15}C_{10}$, at the grain boundaries. The fraction of $Fe_2P_2O_7$ was found to be correlated with degree of Li deficiency. For stoichiometric $LiFePO_4$, formation of phosphides was found at a higher temperature (850 °C). Their investigations also found that formation of iron phosphides could be achieved at lower temperatures and shorter sintering periods using stronger reducing environments such as 7% H_2-N_2 or NH_3 atmospheres.

Similar investigations were carried out by the Masquelier group (Delacourt et al.[8,35]). They found that Li-rich compositions processed at temperatures >500 °C in a N_2 atmosphere consist of $LiFePO_4$, $Li_3Fe_2(PO_4)_3$, and iron oxides. For Li-deficient compositions, the mixed-valence phosphate, $Fe_7(PO_4)_6$, was formed and as the lithium content decreased, less $Fe_7(PO_4)_6$ formed but α-$FePO_4$ appeared. Significant amounts of Li_3PO_4 and iron oxides (Fe_2O_3 and Fe_3O_4) were also found as a result of partial decomposition of $LiFePO_4$.

Kim et al.[36] also reported on the effects of synthesis conditions on the properties of $LiFePO_4$. Their experiments found $Fe_2P_2O_7$ and Li_3PO_4 impurities for Li-deficient and Li-excess stoichiometries, respectively, consistent with the findings of the Nazar and Masquelier groups.

Table 2 summarizes the predicted phase equilibria from our first principles Li−Fe−P−O_2 phase diagrams for three values of μ_{O_2}, which we believe to be representative of the range of oxidation environments in experimental literature. Lower μ_{O_2} phase equilibria correspond to more reducing experimental conditions of higher temperatures and/or lower oxygen partial pressures and/or the presence of reducing agents, and vice versa. Comparing the predicted phase equilibria with the experimental findings, we find the following:

1. Li-Deficient Stoichiometries. At less reducing conditions ($\mu_{O_2} = -10.50$ eV), the predicted phase equilibria for intermediate to severe Li-deficiency compositions is consistent with the formation of $Fe_7(PO_4)_6$ and $FePO_4$ observed by Delacourt et al.[8] $LiFePO_4$ itself is not present in the phase diagram at this μ_{O_2} level and begins to appear only at $\mu_{O_2} = -11.52$ eV (Figure 2). However, inhomogeneities in the reaction environment may allow the coexistence of $LiFePO_4$ with $Fe_7(PO_4)_6$ and $FePO_4$ in actual experiments. At more reducing conditions, the predicted phase equilibria contains $Fe_2P_2O_7$, and under extremely reducing conditions, iron phosphides are formed. This again compares well with the findings of the Nazar group. Their observation that the proportion of $Fe_2P_2O_7$ decreases with more Li-deficient stoichiometries can also be seen from the first principles phase diagrams by way of the lever rule. We note that for highly reducing environments the first principles phase diagrams predict the formation of FeP_4, which is seldom seen under experimental conditions. As mentioned previously, we attribute this to likely errors in the calculated energies of the metallic iron phosphides due to the application of the GGA+U methodology. Furthermore, phosphorus is treated as a condensed phase in our framework, though it is likely the actual experimental conditions are low P chemical potential environments due to the vaporization of P.

2. Li-Rich Stoichiometries. For compositions with slight to intermediate Li excess, the predicted phase equilibria comprises Li_3PO_4 and iron oxides in all but the most extreme reducing conditions. This is consistent with the findings of Kim et al.[36] The formation of $Li_3Fe_2(PO_4)_3$, $LiFePO_4$, and Fe_2O_3 for Li-rich compositions observed by Delacourt et al.[35] may be due to the partial oxidation of $LiFePO_4$ (Figure 2) or minor inhomogeneities in the reactants or reaction environment.

3. Stoichiometric $LiFePO_4$. At sufficiently oxidizing environments, the predicted equilibrium phases are $Li_3Fe_2(PO_4)_3$ and Fe_2O_3. This is consistent with the findings of Belharouak et al.[37]

From Figure 6, we can obtain the predicted temperatures necessary to achieve reduction of $LiFePO_4$ and $Fe_2P_2O_7$ to the iron phosphides. In the absence of reducing agents, the formation of iron phosphides from reduction of $LiFePO_4$ is predicted to occur at >1500 K. In the presence of carbon, however, the predicted transition temperature decreases to around 1100 K (assuming CO is produced at the reference partial pressure), while in a H_2 atmosphere, the predicted transition temperature is even lower at around 900 K (again assuming H_2 and H_2O are at the reference partial pressure). For formation of the iron phosphides from $Fe_2P_2O_7$, the phase diagrams indicate that this happens through a two-stage reduction where $Fe_2P_2O_7$ decomposes first to $Fe_3(PO_4)_2$, which is in turn reduced to the iron phosphides. The latter

(35) Delacourt, C.; Poizot, P.; Tarascon, J. M.; Masquelier, C. *Nat. Mater.* **2005**, *4*, 254–260.
(36) Kim, D. K.; Park, H. M.; Jung, S. J.; Jeong, Y. U.; Lee, J. H.; Kim, J. J. *J. Power Sources* **2006**, *159*, 237–240.
(37) Belharouak, I.; Johnson, C.; Amine, K. *Electrochem. Commun.* **2005**, *7*, 983–988.

process is predicted to take place at slightly lower temperatures than that for reduction of $LiFePO_4$.

Comparing with the experimental literature, the following observations can be made:

1. The predicted temperatures for C/CO-CTR of $LiFePO_4$ compare well with those in experimental literature, which are generally in the range of 800–900 °C (1073–1173 K).

2. Herle et al.[7] have observed that $LiFePO_4$ samples synthesized from non-carbon-containing precursors do not become electrically conducive at any of the temperatures investigated. This is consistent with the high thermal reduction temperatures predicted for stoichiometric $LiFePO_4$ in the absence of reduction agents.

3. Ellis et al.[11] have reported that CTR of $Fe_2P_2O_7$ to iron phosphides takes place at around 800 °C, compared with 850 °C for $LiFePO_4$. Reduction in a 7% H_2-N_2 atmosphere was found to take place at an even lower temperature and shorter sintering times. These are again consistent with the predictions from our modified Ellingham diagram.

Overall, we found that the predicted phase equilibria and transition temperatures from our first principles phase diagram and modified Ellingham diagram agree remarkably well with the findings in the experimental literature surveyed. While there are some differences in some of the phases and temperatures predicted, these errors do not seem to affect in a significant way the phase evolution as function of composition or reduction conditions.

4.2. Potential Applications. Having validated the diagrams with experimental literature, they can be used to evaluate current approaches to synthesizing $LiFePO_4$ and in the development of new synthesis routes to achieve desired properties.

Yamada et al.[38] identified two key challenges to achieving optimal performance for $LiFePO_4$: (i) undesirable particle growth at $T > 600$ °C and (ii) the presence of residual noncrystalline Fe^{3+} phase at $T < 500$ °C. Based on our literature survey, current approaches to addressing these obstacles seem to primarily focus on tuning the oxidation environment and Li off-stoichiometry. Indeed, our phase diagrams show that the nature and degree of Li off-stoichiometry are important factors in influencing the eventual phase equilibria obtained. For instance, an excess of lithium is often introduced during $LiFePO_4$ synthesis to compensate for lithium volatility at high-temperature firing conditions. As can be seen from Figures 2−4, a Li-excess stoichiometry is likely to result in the formation of undesirable iron oxides at low temperatures, while higher temperatures may lead to excessive particle growth. The phase diagrams provide a means to identify possible phase equilibria which may offer better performance. Applying the lever rule on the phase diagrams also provides a means to determine the stoichiometric proportions needed to achieve a desired balance of $LiFePO_4$ and impurity phases, and the modified Ellingham diagram provides a method for fine-tuning the chemical and physical environments to achieve the desired degree of reduction of $LiFePO_4$ and impurity phases.

While our main motivation for this work is to apply the phase diagrams to $LiFePO_4$ synthesis, this is by no means the only phase of interest in the $Li-Fe-P-O_2$ system. For example, iron phosphates, in particular $FePO_4$, have been used as a catalyst for oxidative dehydrogenation reactions for many years[39] while Li_3PO_4 is used as a solid electrolyte in film batteries. The phase diagrams developed can be provide a better understanding of redox phase relations for these phases.

Beyond the $Li-Fe-P-O_2$ system, the general methodology demonstrated in this paper can be extended to any system of interest with similar characteristics, i.e., systems with primarily solid state phase transitions in response to changes in the chemical potential of a gas.

4.3. Limitations. Several limitations are inherent in our approach to determine the phase diagrams.

First, our phase diagram is developed from phases in the $Li-Fe-P-O_2$ system reported in the ICSD database. Our analysis, therefore, by definition does not include phases which have not yet been discovered. However, we do not foresee this to be a major issue as the $Li-Fe-P-O_2$ system is a well-studied system, and most of the relevant phases should have already been identified. A more elaborate search for unknown compounds would require a method to predict likely crystal structures for a large number of possible stoichiometries. While such an approach has been developed for metals,[40] it does not yet exist for oxides.

Second, we have made several key assumptions in our free energy model, most notably considering only the entropic contributions of gaseous phases. This assumption seems reasonable for the phase equilibria we are interested in, where phase transitions consist primarily of solid state changes with the absorption or release of gases. It should be noted, however, that the predicted transition temperatures are likely to be overestimated as the entropy terms we neglected in the solid state would lower their free energy somewhat.

Finally, while the GGA+U methodology chosen for our DFT computations has been shown to be useful in obtaining accurate redox energies, the appropriate values of $U_{\text{effective}}$ are dependent on the crystal environment and valence state of the transition metal ion. We have used an average $U_{\text{effective}}$ for Fe in valence states ranging from 0 to 3+. This is likely to result in errors in the calculated energies, particularly for the strongly reduced states.

5. Conclusion

In this work, we have presented an efficient method of characterizing from first principles the phase diagram of the $Li-Fe-P-O_2$ system as a function of oxidation conditions. As we only consider the entropy of gaseous phases, temperature and oxygen partial pressure can be put on the same scale. By incorporating experimental thermodynamic data, we were also able to construct a modified Ellingham diagram

(38) Yamada, A.; Chung, S. C.; Hinokuma, K. *J. Electrochem. Soc.* **2001**, *148*, A224–A229.

(39) Miller, J. E.; Gonzales, M. M.; Evans, L.; Sault, A. G.; Zhang, C.; Rao, R.; Whitwell, G.; Maiti, A.; King-Smith, D. *Appl. Catal., A* **2002**, *231*, 281–292.

(40) Fischer, C. C.; Tibbetts, K. J.; Morgan, D.; Ceder, G. *Nat. Mater.* **2006**, *5*, 641–6.

to provide a visual representation of the relation between the temperatures, oxygen partial pressures, and chemical environment necessary to achieve a desired reduction reaction. The predicted phase equilibria and reduction temperatures compare well to experimental findings on stoichiometric and off-stoichiometric $LiFePO_4$ reactions. We believe that the combined application of the phase diagrams and Ellingham diagram provides a means to more efficiently focus experimental efforts to optimize synthesis approaches for $LiFePO_4$. While we have focused on the synthesis of $LiFePO_4$ in this work, the phase diagram can be applied to study other compounds of interest in the same system, and more generally, the methodological approach developed can conceivably be extended to any system of interest.

Acknowledgment. This work was supported by the U.S. Department of Energy under Contract DE-FG02-96ER45571 and the BATT program under Contract DE-AC02-05CH11231.

CM702327G